Electronic Supplementary Material (ESI) for Journal of Materials Chemistry A.

Supporting Information

A Novel Asymmetrical Multilayered Composite Electrolyte for High-performance Ambient-temperature All-solid-state Lithium Batteries

Zhen Wang, [a] Jiewen Tan, [a] Jiawu Cui, [a] Keyu Xie, [b] Yunfei Bai, [c] Zhanhui Jia, [d] Xiangwen Gao, *[e] Yuping Wu, [f] Wei Tang *[a]

Experimental Section

1.1 Preparation of the asymmetrical multilayered composite Electrolyte

Before preparing the composite electrolyte, PEO (Mv = 6×10^5 g mol^{-1}, Aladdin), PPC (Sigma-Aldrich) and LiTFSI were vacuum dried overnight at 70°C. The particle size of the used LLZTO particles (99.99%, MTI-kejing) was about 500 nm. Firstly, to prepare the SCE membrane which contains 70wt% LLZTO and 30wt% PEO, the PEO (600 mg) and LiTFSI (392 mg) were precisely measured and introduced into 8 mL of anhydrous acetonitrile (ACN, Sigma-Aldrich). The mixture was subjected to continuous stirring at 60°C for a duration of 8 hours. After that, LLZTO(1400mg) was introduced into the solution. In order to maintain the uniform distribution of particles, LLZTO was introduced into the prepared PEO solution with continuous stirring at 80°C for overnight, following by ultrasonically dispersed for 1 h before casting. The scale bar for the all horizontal cross section images of TOF-SIMS is 100 × 100 μm. The asymmetric multilayer composite electrolyte was prepared using the same method layer by layer. An argon-filled glovebox with an H_2O and O_2 concentration of 0.1 ppm was used for all operations.

1.2 Characterizations

A scanning electron microscope (TESCAN MAIA3 LMH) was used to examine the morphology of MSCE, SCE, PPC, and PEO surfaces and cross-sections. The cross-section samples were obtained through liquid nitrogen quenching. TOF-SIMS characterization analysis was performed using a TOF-SIMS 5-100 spectrometer (ION-TOF GmbH). Analysis chamber was maintained under ultra-high vacuum conditions of 2×10^{-9} mbar. A 2k eV Cs^+ ion beam (sputtering rate estimated at ~0.03 nm s^{-1}) was used for depth analysis of the LFP cathode with a sputtered area of 300 × 300 μm. X-ray photoelectron spectroscopy (XPS, AXIS-ULTRADLD-600W) was performed to characterize the compositions of Li anode surface with depth profiles. All the testing procedures of XPS are strictly insulated from air. The chemical composition information was characterized with Fourier-transform infrared (FTIR) spectrometer (Nicolet iS50) in the range of 4000 – 400 cm^{-1}.

1.3 Electrochemical tests

To measure ionic conductivity, SCE was sandwiched by two stainless steel (SS) electrodes, and tested by Princeton electrochemical workstation at from 30 to 80°C. The stability of SCE under high voltage was characterized by the SS/SCE/Li cell using linear sweep voltammetry (LSV). The LFP (1 C=170 mAh g^{-1}) and NCM622 (1 C=160 mAh g^{-1}) cathodes were prepared by mixing LFP/NCM622 particles, Super P, and polyvinylidene fluoride (weight ratio: 7:2:1) in N-methylpyrrolidone solvent. The mixture was then coated onto aluminum foil. The LFP/MSCE/Li and NCM622/MSCE/Li 2032-type coin cells were constructed with Li metal as the anode and the cathode active materials loading was approximately 1.2 mg cm^{-2}. The assembled cells were activated at 80°C for 8h before test.

Experimental details for measuring the ionic conductivity of MSCE: Firstly, to initiate the activation process, the prepared MSCE was placed between a stainless steel (SS) electrode and a lithium electrode, with the PPC side facing the lithium. The assembled cell was then subjected to an activation process at 80°C for 8 hours. After activation, the cell was immediately disassembled and reassembled into a stainless steel symmetric cell. Subsequently, the cell was tested using a Princeton electrochemical workstation at temperature ranging from 30 to 80°C to get electrochemical impedance spectroscopy.

Discussion

The close contact between the CEI/cathode and SEI/anode during cycling should be attributed to the unique composition and structure of the as-formed interfacial films on cathode and anode and discussed as follow.

Firstly, the 3D rendered images and chemical-depth profiles of organic species in Fig. 3b and 3c illustrate the formation of a compact and thin CEI film (about 8nm thick) on the LFP cathode paired with the PEO-SCE. Additionally, the impedance analysis in Fig. S7 demonstrates that such a dense and thin CEI film can consistently keep close contact with cathode which enhances the fast Li^+ diffusion through the interface. What' more, the intact and well-structured LFP/PEO-SCE interface after cycling in Fig. 3a also suggests that the in-situ generated CEI film is beneficial for protecting and maintaining close contact with the cathode particles during the long cycling, which should be attributed to the unique organic and inorganic species distributions, such as LiF, Fe metal fluoride/oxide and P-containing components in the CEI film on the LFP cathode paired with the PEO-SCE (Figure 3f and S12-17).[1]

On the other hand, the in-depth XPS analysis in Fig. 4d-f demonstrates that the SEI derived with SCE-PPC contains more PPC-derived products, Li_2CO_3 and LiF due to the "self-sacrifice" of PPC. The Li_2CO_3 species distributed in the outer layer of SEI (Fig. S24a) can effectively hinder the further decomposition of the electrolyte and ensure the stability of the SEI during long cycling.[1] Furthermore, the preferable presence of $ROCO_2Li$ and ROLi in the inner layer of SEI (Fig. S24a and b) can help wet the interface and construct close interfacial contact between the electrolyte/anode, as evidenced by the dramatic decrease in interfacial resistance and close contact of SCE-PPC with Li after activation.[2-4]

Last but not the least, a LiF-rich SEI film is in-situ generated on Li anode and concentrates in the inner layer of SEI (Fig. S24c), which can induce the uniform deposition of Li and hinder the growth of Li dendrites and inhibit the irreversible reaction after cycling (Fig. S25).[5-6]

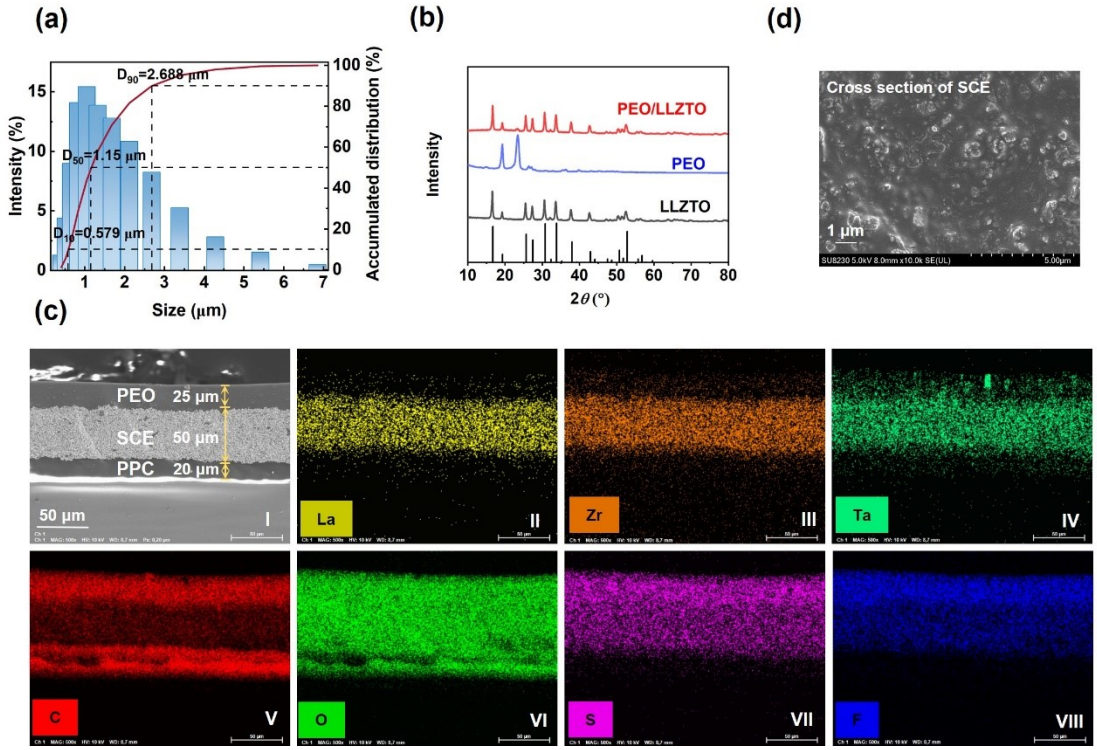

Figure S1. a) Size distribution of pristine LLZTO particles. b) XRD patterns of the as-prepared PEO, LLZTO and PEO. c) SEM images of MSCE with hierarchical structure (I), EDS mapping of MSCE, the elements of lanthanum (II), zirconium (III), tantalum (IV), carbon (V), oxygen (VI), sulfur (VII) and fluorine (VIII). d) The cross-sectional SEM image of SCE.

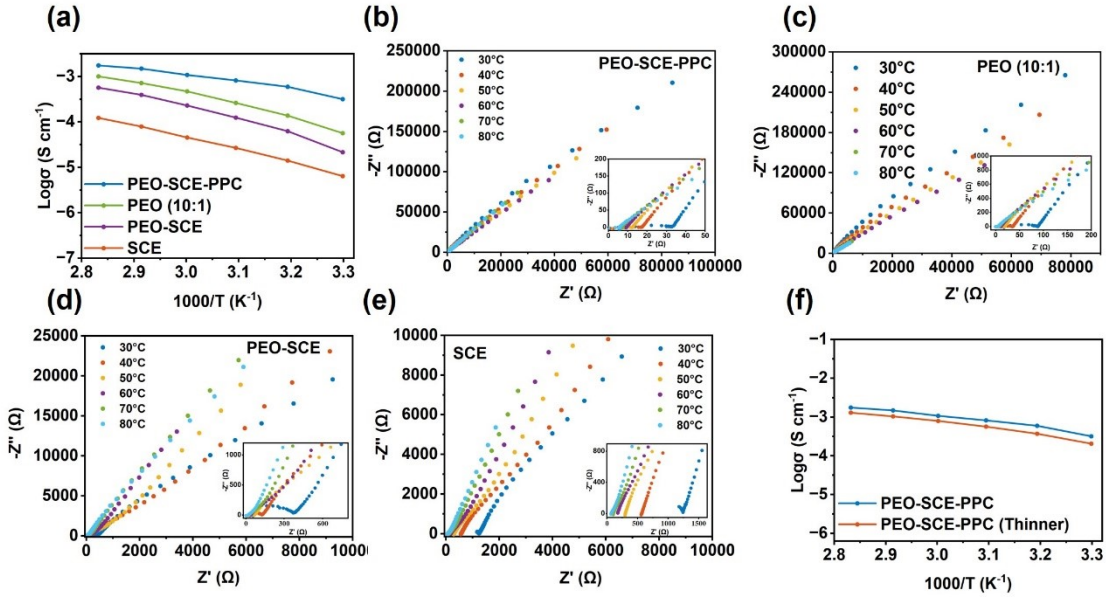

Figure S2. a) Temperature dependent ionic conductivity of PEO (10:1), SCE, PEO-SCE and PEO-SCE-PPC; Electrochemical impedance spectroscopy (EIS) comparison of b) reassembled activated SS/PEO-SCE-PPC/SS , c) SS/PEO (10:1)/SS, d) SS/PEO-SCE/SS, e) SS/SCE/SS cell, f) Temperature dependent ionic conductivity of PEO-SCE-PPC and PEO-SCE-PPC (thinner).

Table S1. The ionic conductivity data of SCE, PEO-SCE, PEO-SCE-PPC, PEO (10:1) and PEO-SCE-PPC (Thinner)

Ionic conductivity [S cm^{-1}]	SCE	PEO-SCE	PEO-SCE-PPC	PEO (10:1)	PEO-SCE-PPC (thinner)
30°C	6.42×10^{-6}	2.15×10^{-5}	3.21×10^{-4}	5.71×10^{-5}	2.06×10^{-4}
40°C	1.43×10^{-5}	6.27×10^{-5}	5.95×10^{-4}	1.39×10^{-4}	3.73×10^{-4}
50°C	2.71×10^{-5}	1.24×10^{-4}	8.28×10^{-4}	2.64×10^{-4}	5.67×10^{-4}
60°C	4.58×10^{-5}	2.30×10^{-4}	1.09×10^{-3}	4.71×10^{-4}	7.96×10^{-4}
70°C	7.96×10^{-5}	3.98×10^{-4}	1.50×10^{-3}	7.25×10^{-4}	1.04×10^{-3}
80°C	1.22×10^{-4}	5.69×10^{-4}	1.77×10^{-3}	1.01×10^{-3}	1.30×10^{-3}

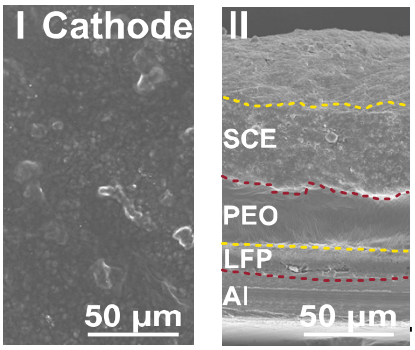

Figure S3. Typical surface morphologies of the LFP cathode and Cross-section SEM images of LFP/MSCE obtained from the LFP/MSCE/Li battery after 10 cycles at 0.1C at 40°C.

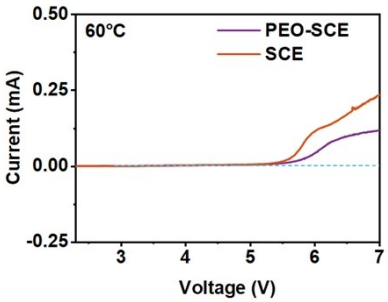

Figure S4. LSV for SCE and PEO-SCE at 60 °C with a scan rate of 10 mV s^{-1}.

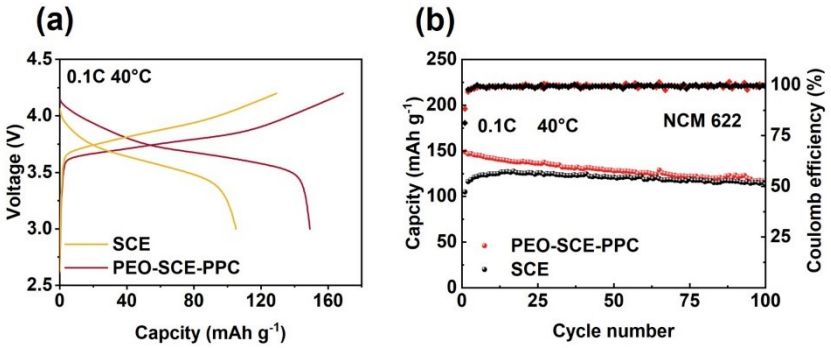

Figure S5. a) Charge–discharge curves and b) cycling performance of NCM622//Li batteries using SCE and PEO-SCE-PPC.

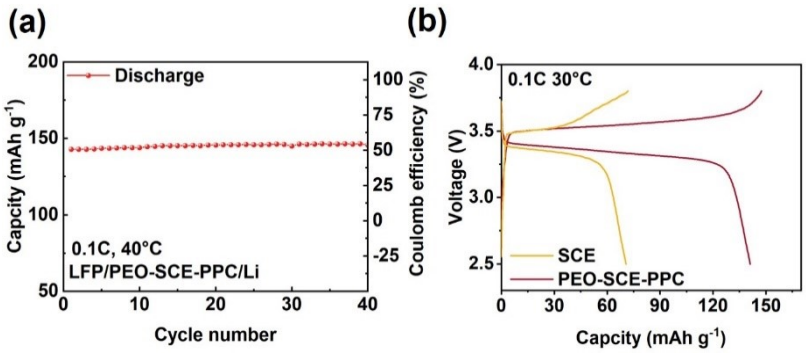

Figure S6. a) Cycling performance of LFP/MSCE/Li pouch cells at 40°C. b) Charge−discharge curves of LFP//Li batteries using SCE and PEO-SCE-PPC at 30°C.

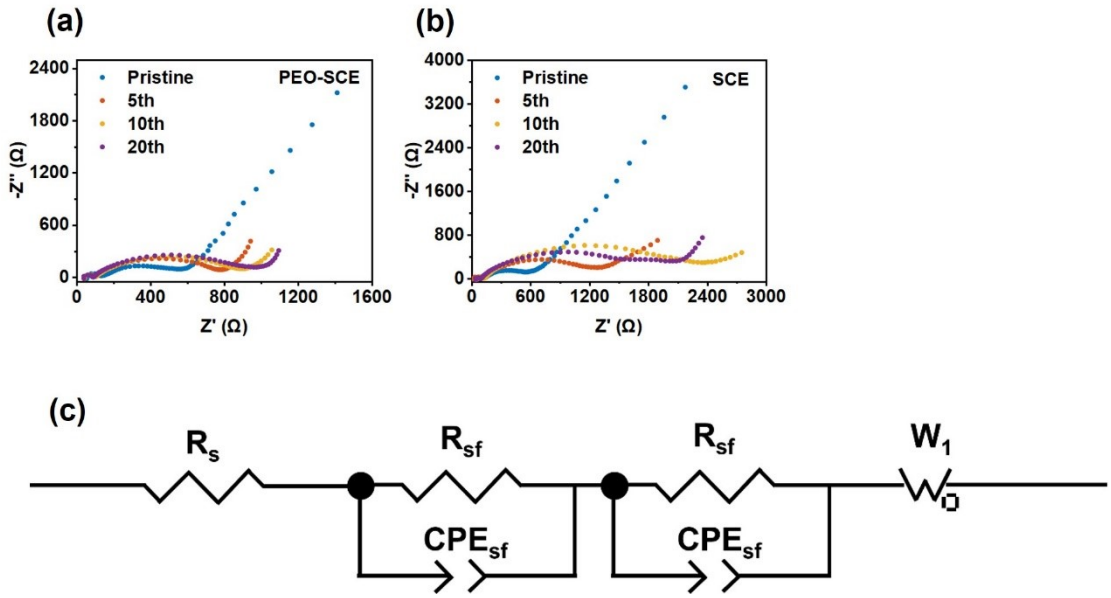

Figure S7. EIS of the LFP/Li batteries using a) PEO-SCE and b) SCE after different cycles at 0.1C. c) The equivalent circuit used to fit the impedance data.

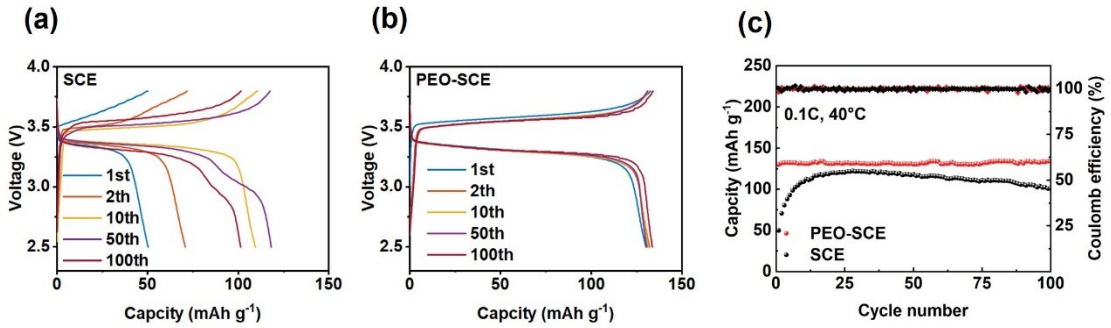

Figure S8. a) Charge−discharge curves of LFP/SCE/Li at 40°C. b) Charge−discharge curves of LFP/PEO-SCE/Li at 40°C. c) Cycling performances of LFP//Li batteries using SCE and PEO-SCE.

Table S2. Impedance parameters for LFP/Li batteries using PEO-SCE and SCE electrolyte.

Sample	PEO-SCE			SCE		
Impedance [Ω]	R_s	R_{sf}	R_{ct}	R_s	R_{sf}	R_{ct}
Original	72.54	40.79	473.6	46.48	54.86	341.4
After 5 cycles	60.61	28.41	698.1	21.38	29.68	902.9
After 10 cycles	53.53	34.8	731.9	47.71	48.65	1927
After 20 cycles	51.01	29.66	778.5	46.6	31.6	1590

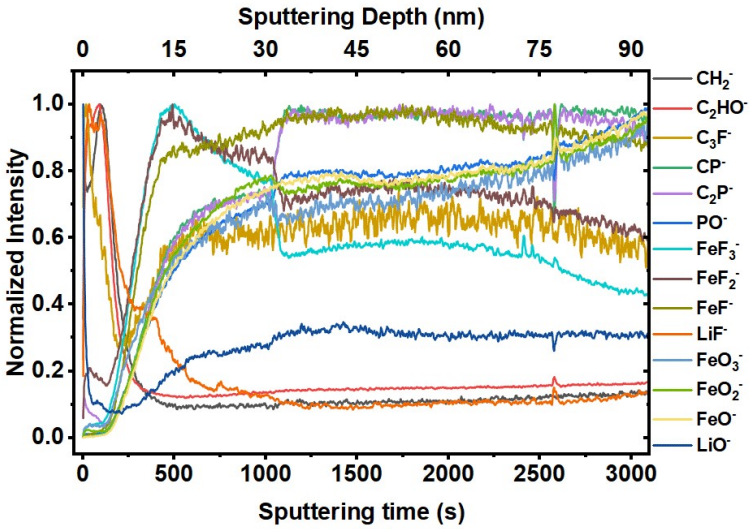

Figure S9. The normalized depth profiling of several secondary ion fragments of interest on the surface of the cycled LFP cathode in the PEO-SCE electrolyte after 10 cycles at 0.1 C.

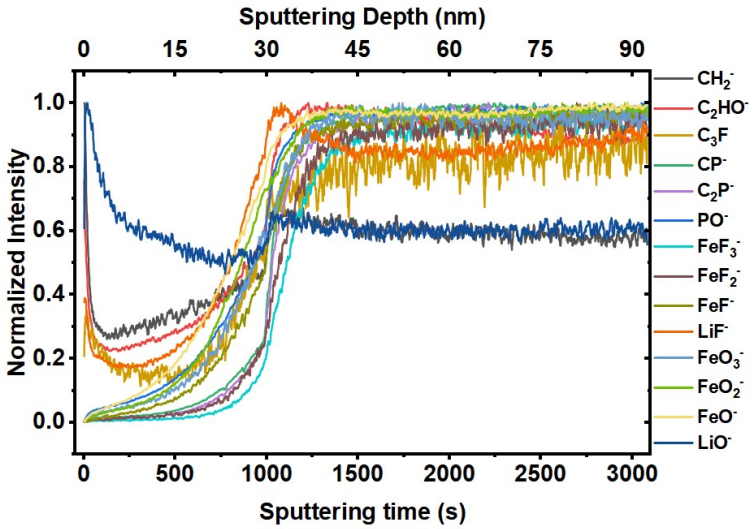

Figure S10. The normalized depth profiling of several secondary ion fragments of interest on the surface of the cycled LFP cathode in the SCE electrolyte after 10 cycles at 0.1 C.

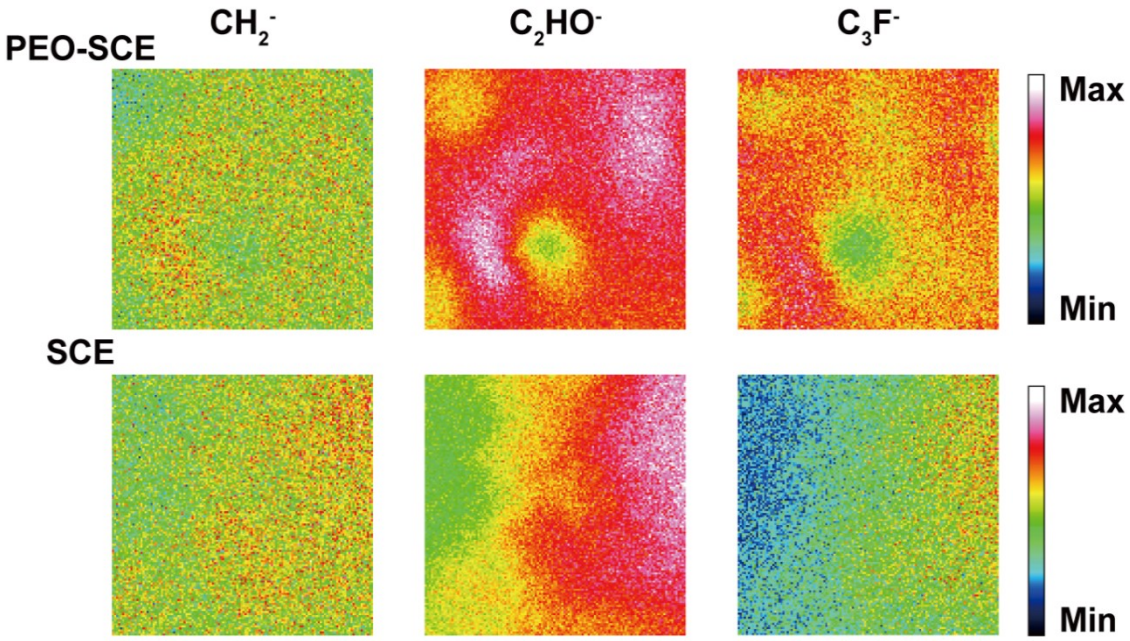

Figure S11. TOF-SIMS chemical imaging of CH_2^-, C_2HO^- and C_3F^- species on the cycled LFP cathode surface with PEO-SCE and SCE (based on TOF-SIMS test data of a diagram).

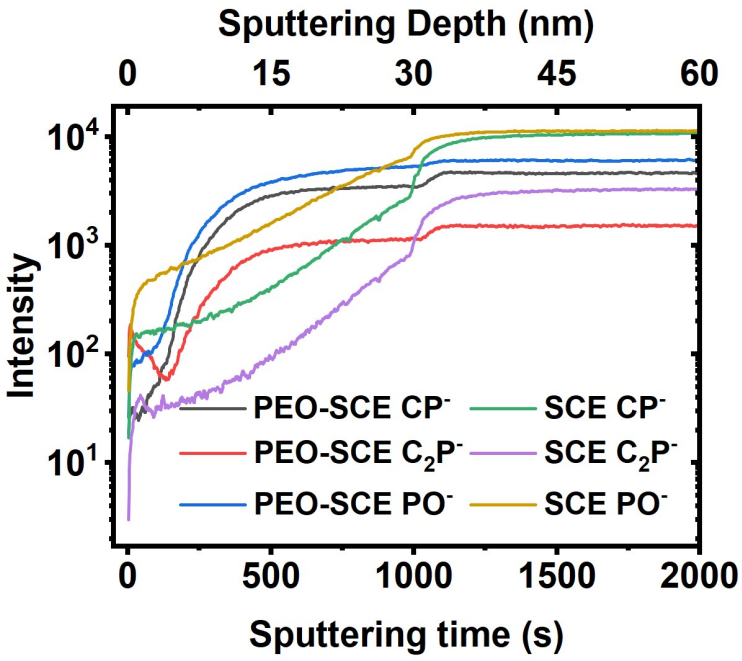

Figure S12. TOF-SIMS depth profiles of CP^-, C_2P^- and PO^- on the cycled LFP cathode surface with PEO-SCE and SCE.

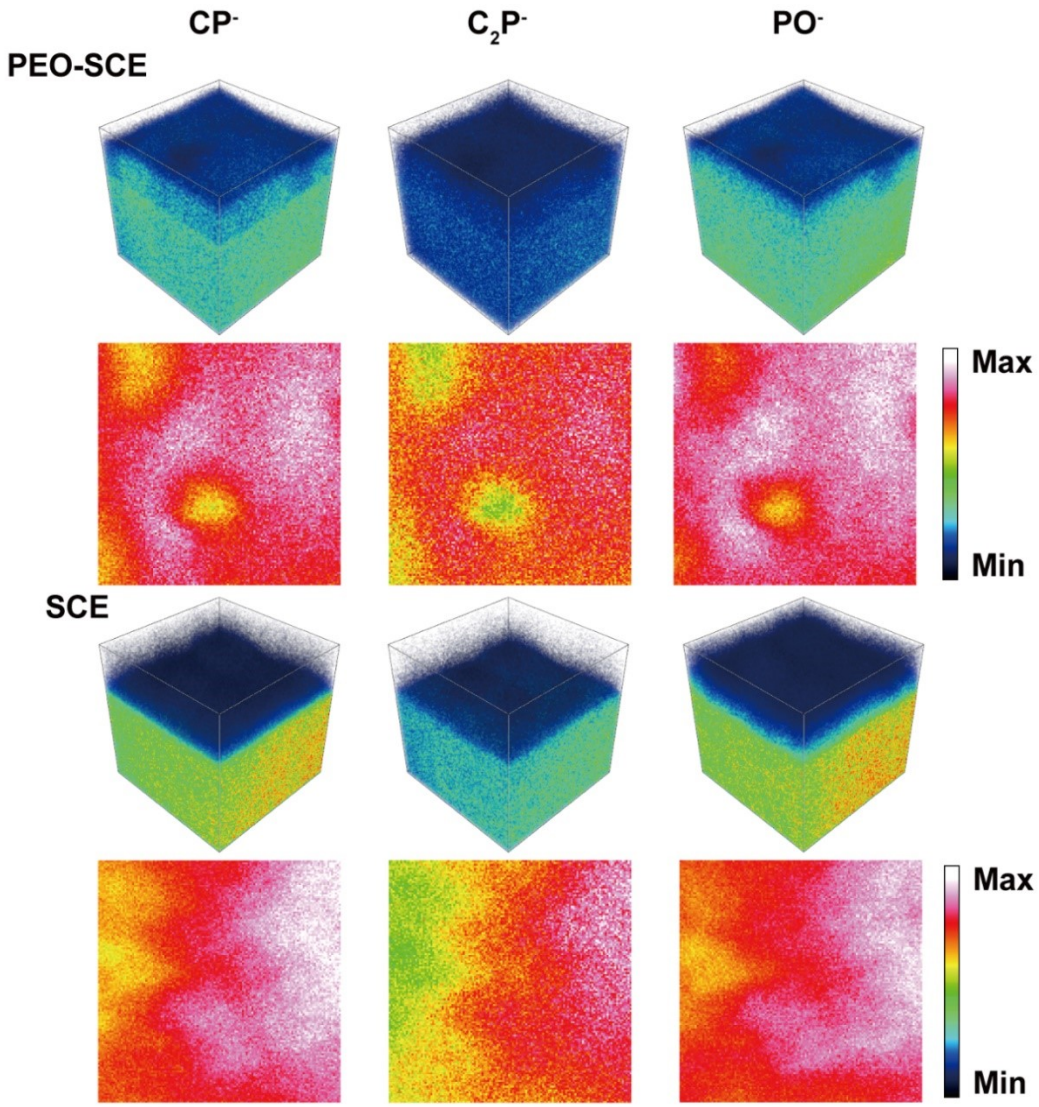

Figure S13. 3D render of the composites (CP^-, C_2P^- and PO^-) concentration distribution on the cycled LFP cathode surface with PEO-SCE and SCE (based on TOF-SIMS test data of a diagram).

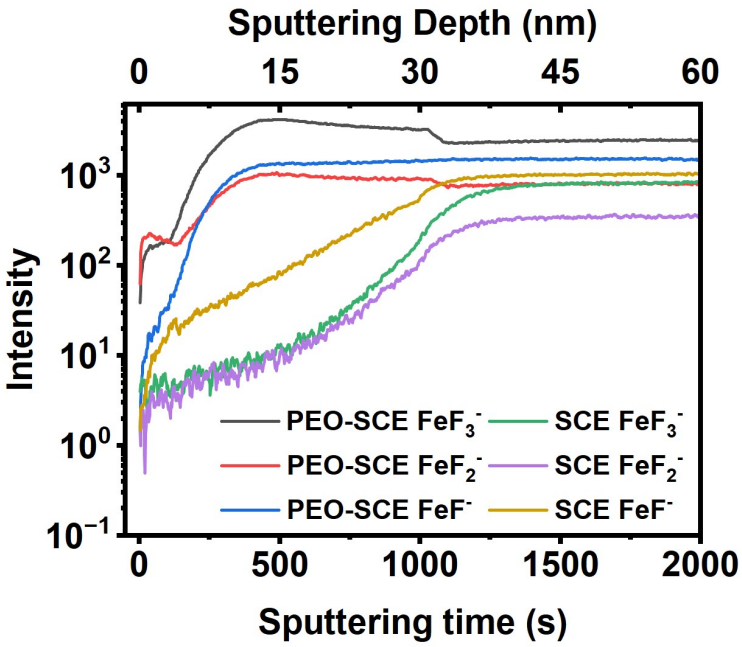

Figure S14. TOF-SIMS depth profiles of FeF_3^-, FeF_2^- and FeF^- on the LFP cathode surface with PEO-SCE and SCE.

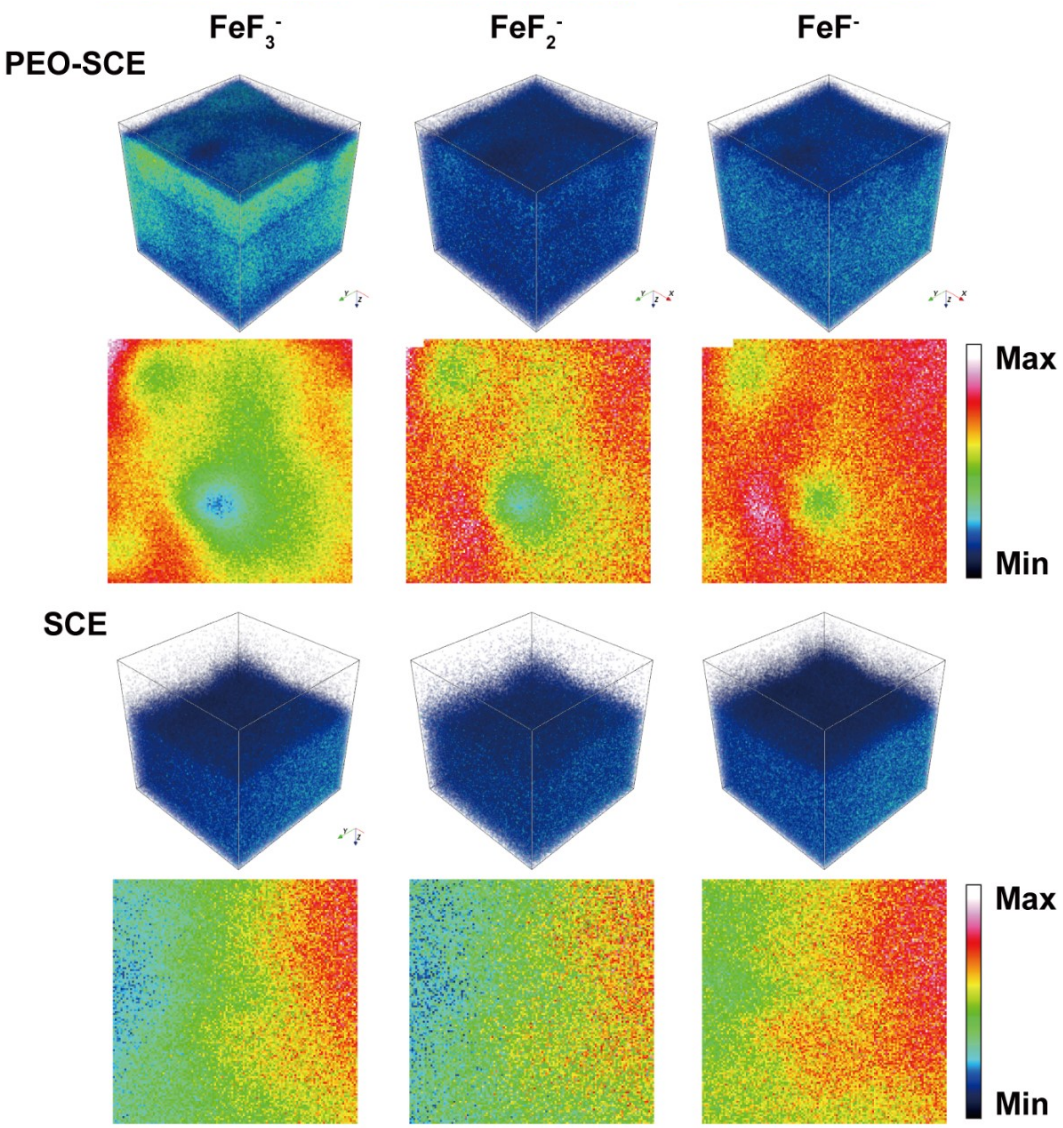

Figure S15. 3D render of the composites (FeF_3^-, FeF_2^- and FeF^-) concentration distribution on the cycled LFP cathode surface with PEO-SCE and SCE (based on TOF-SIMS test data of a diagram).

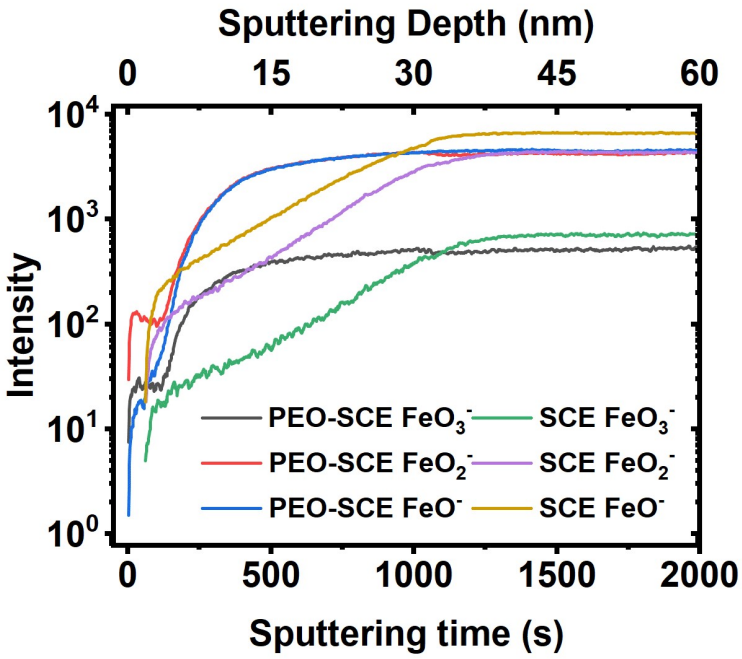

Figure S16. TOF-SIMS depth profiles of FeO_3^-, FeO_2^- and FeO^- on the LFP cathode surface with PEO-SCE and SCE.

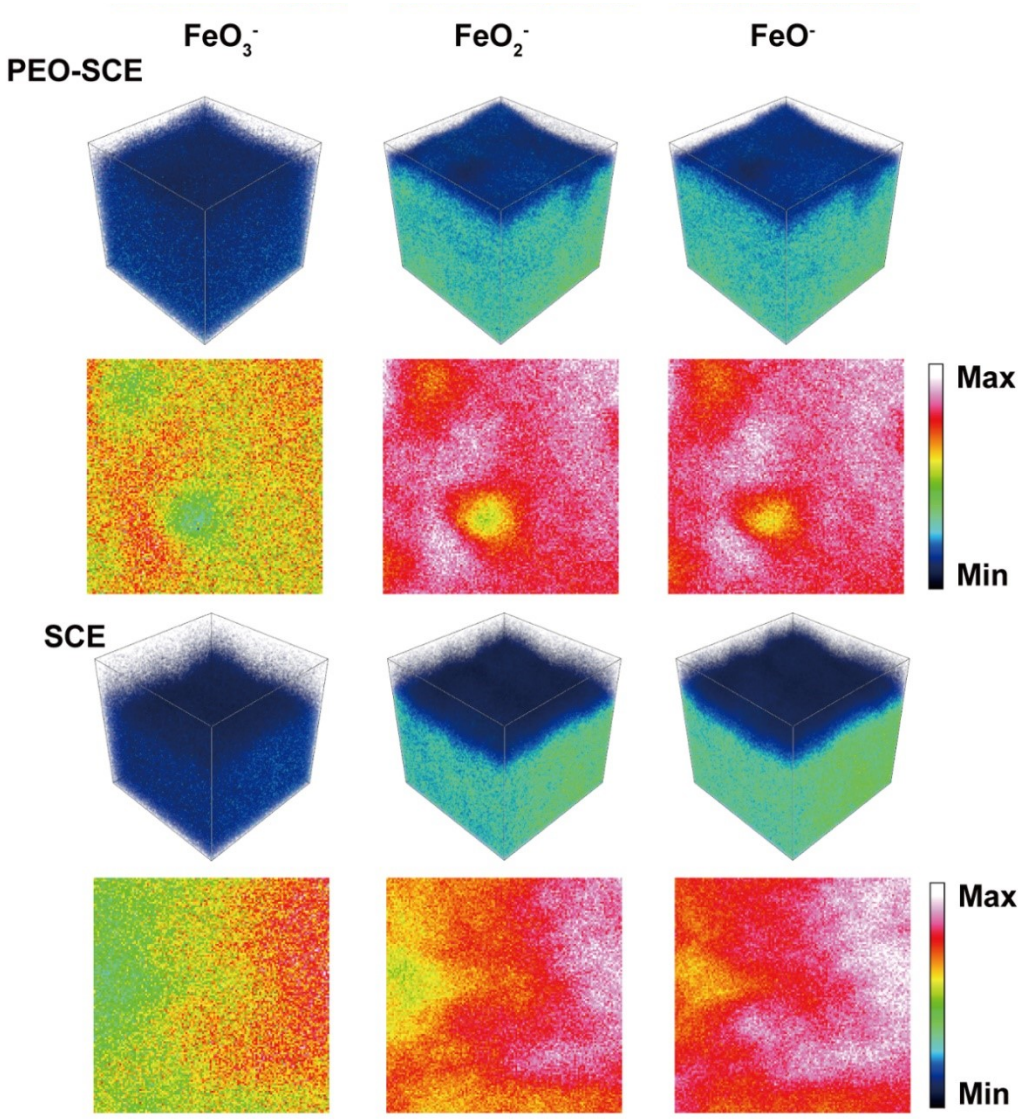

Figure S17. 3D render of the composites (FeO_3^-, FeO_2^- and FeO^-) concentration distribution on the cycled LFP cathode surface with PEO-SCE and SCE (based on TOF-SIMS test data of a diagram).

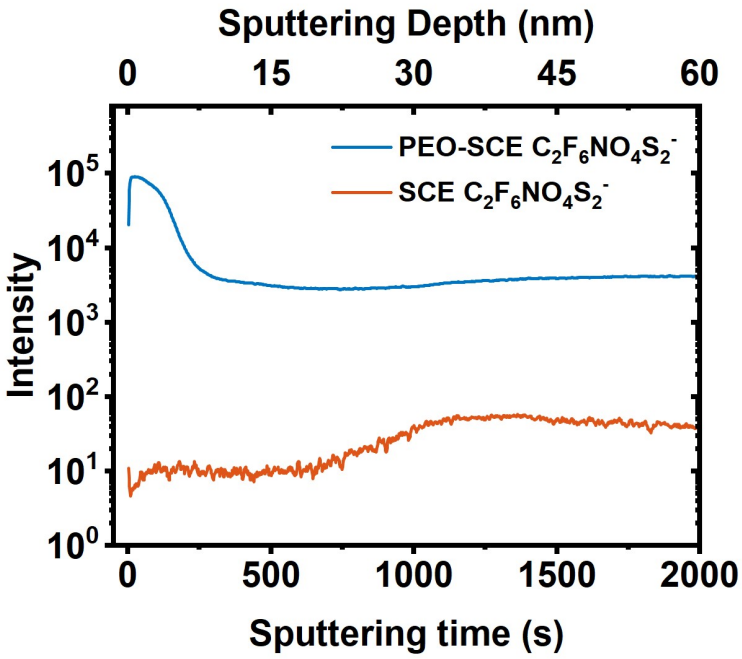

Figure S18. TOF-SIMS depth profiles of $C_2F_6NO_4S_2^-$ on the cycled LFP cathode surface with PEO-SCE and SCE.

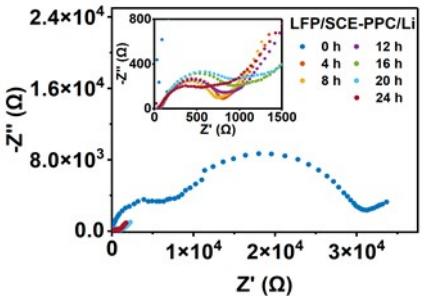

Figure S19. EIS of the LFP/SCE-PPC/Li cell during the activation process at 80 °C.

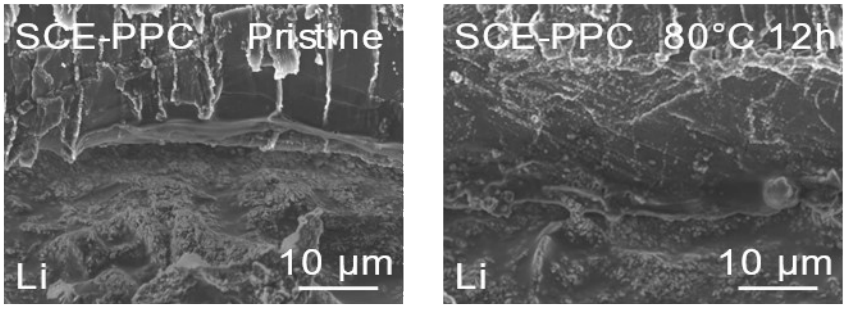

Figure S20. Typical SEM images of the contact interface between SCE-PPC and Li-metal electrode before and after activation.

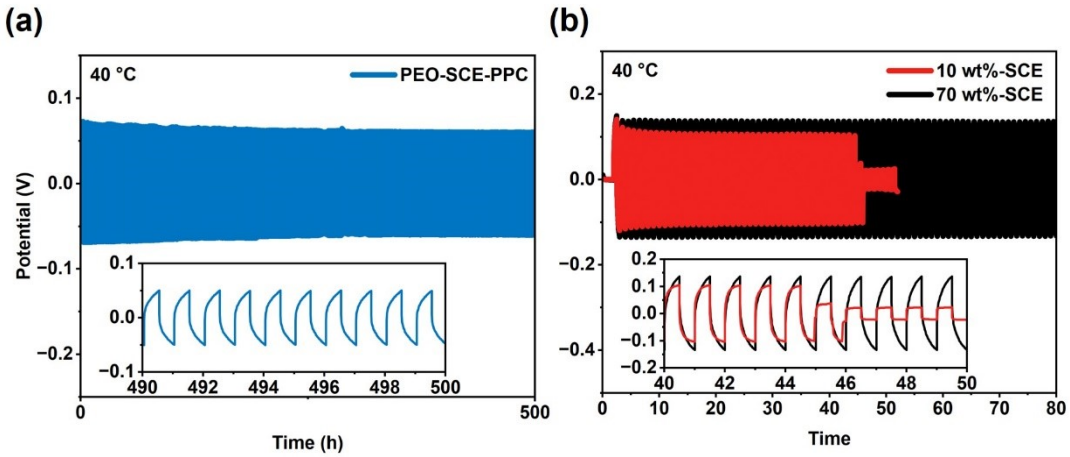

Figure S21. Voltage profiles of the continued lithium plating/stripping cycling of symmetric cells with a) PEO-SCE-PPC, b) 10 wt% LLZTO -SCE and 70 wt% LLZTO -SCE at current density of 0.05 mA cm^{-2}.

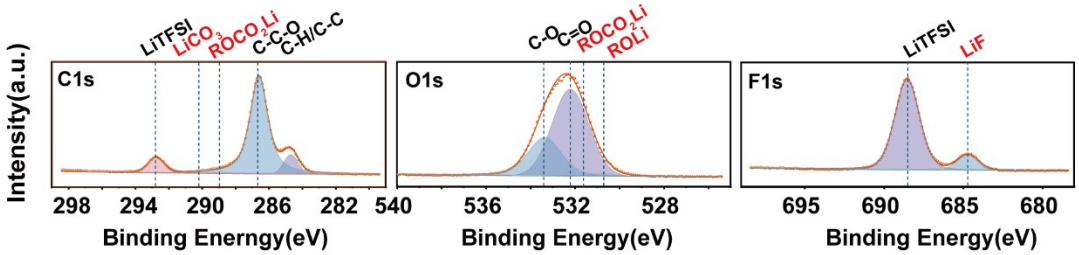

Figure S22. C 1s, O 1s and F 1s XPS spectra of the cycled Li anode surface obtained from Li/SCE/Li symmetrical battery after 10 cycles.

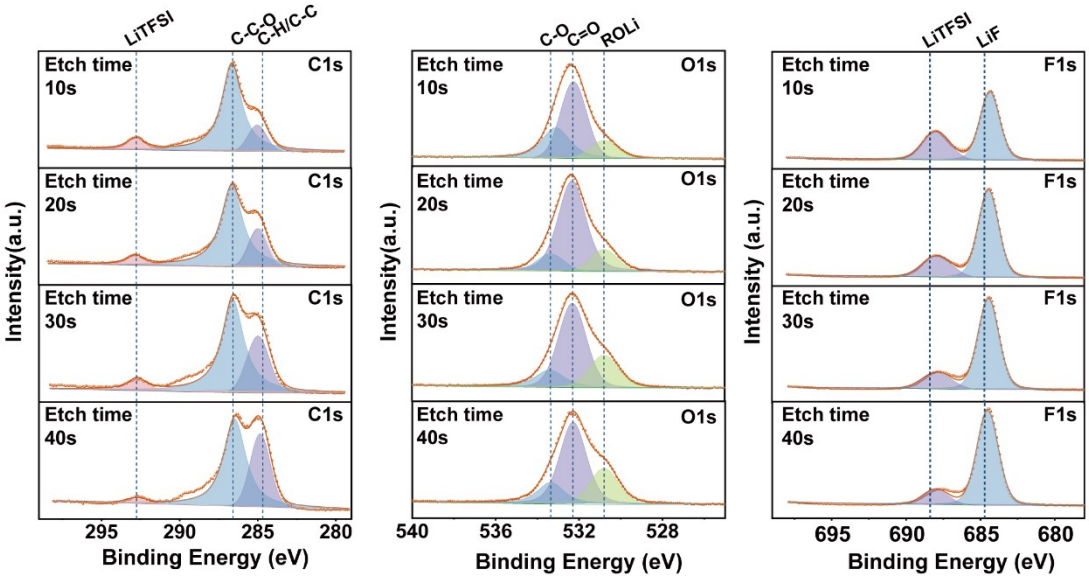

Figure S23. C 1s, O 1s and F 1s in-depth XPS spectra at various etching time of 10, 20,30 and 40s on the Li metal surface obtained from Li/SCE/Li symmetrical battery after 10 cycles.

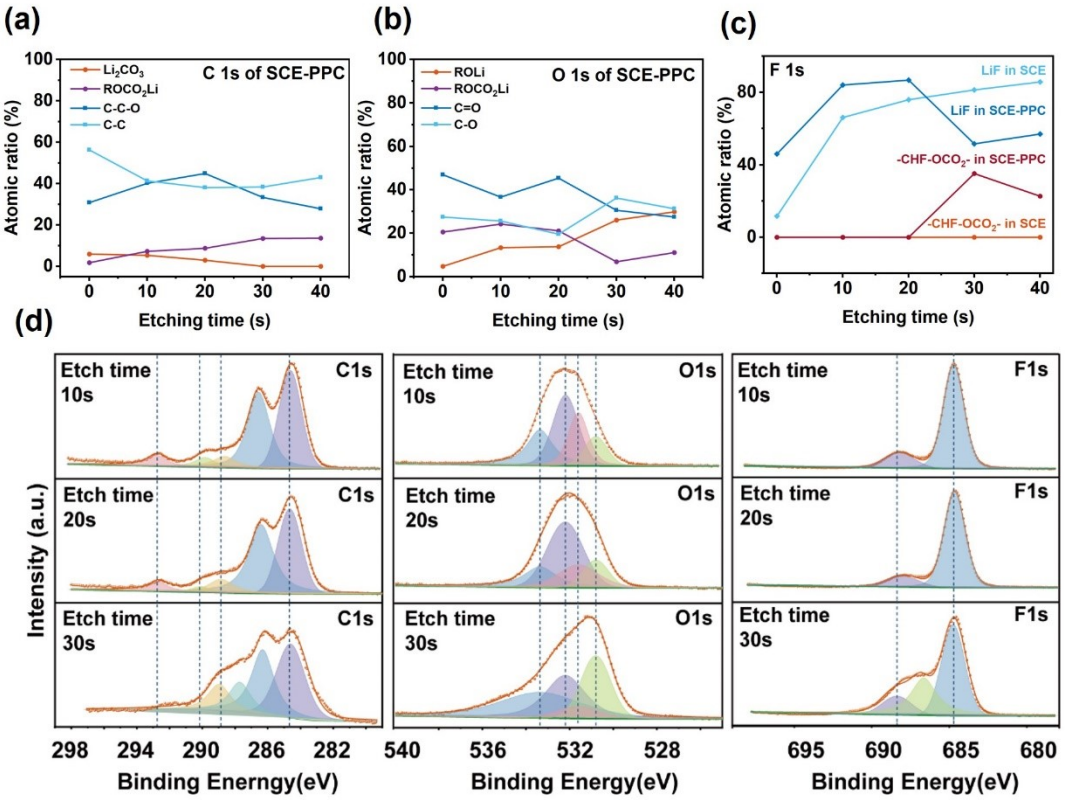

Figure S24. The atomic composition ratios by XPS measurement of the SEI film formed on the Li anode of a) C 1s, b) O 1s and c) F1s. d) C 1s, O 1s and F 1s in-depth XPS spectra at various etching time of 0, 10, 20,30 and 40s on the Li metal surface obtained from Li/SCE-PPC/Li symmetrical battery after 10 cycles.

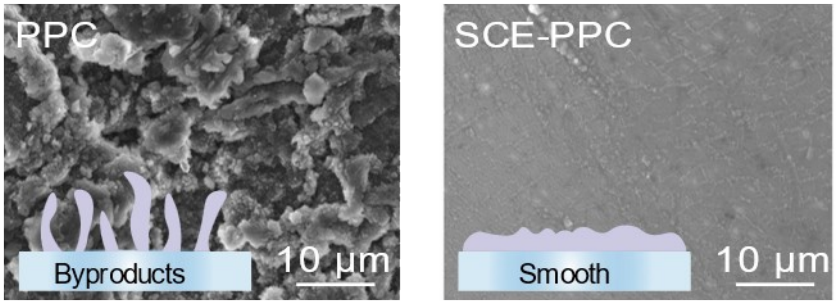

Figure S25. SEM images of typical surface morphologies of the Li anode cycled after 100 cycles with PPC and SCE-PPC.

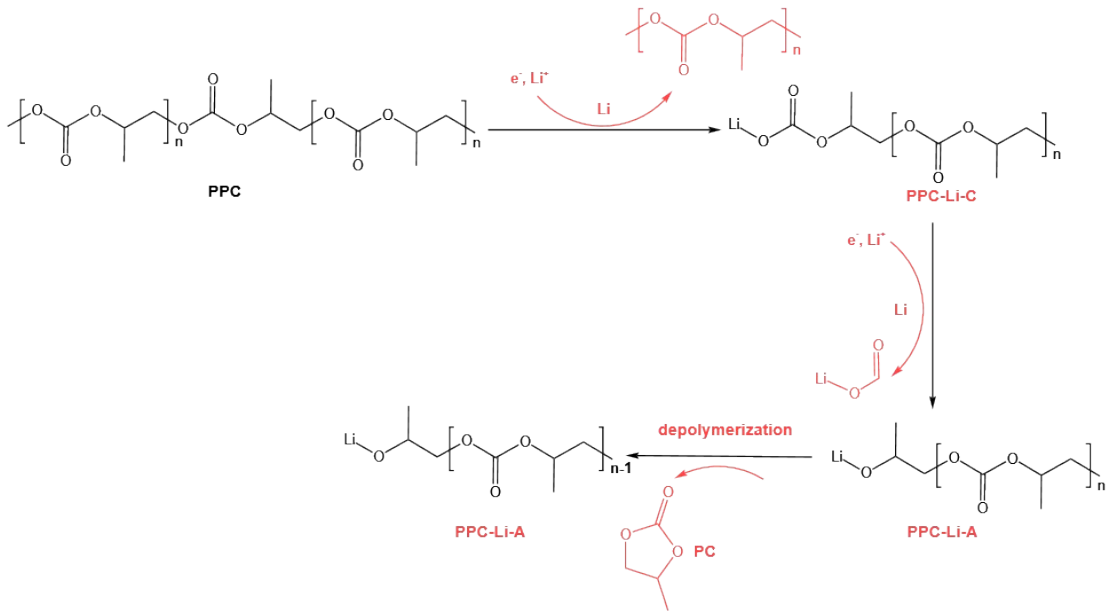

Figure S26. Schematic diagram of the PPC “self-sacrifice” process.

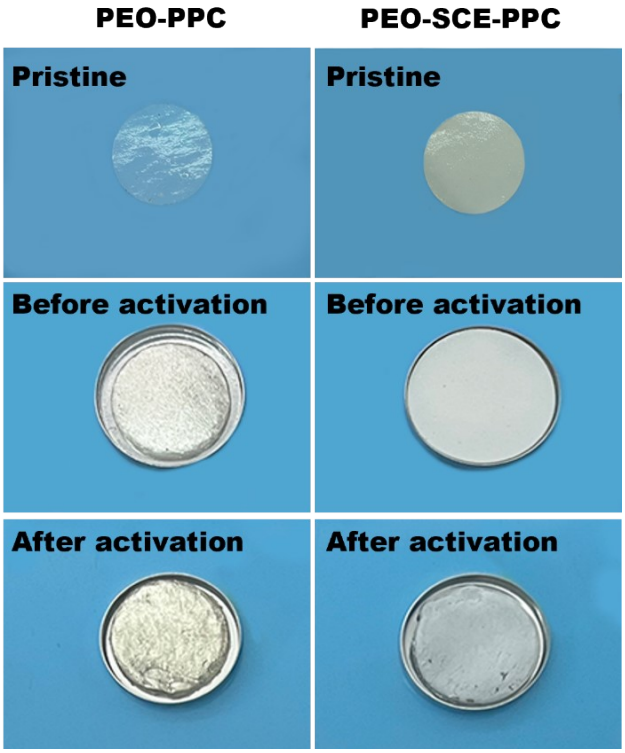

Figure S27. Digital images of PEO-PPC and PEO-SCE-PPC before and after activation process at 80°C.

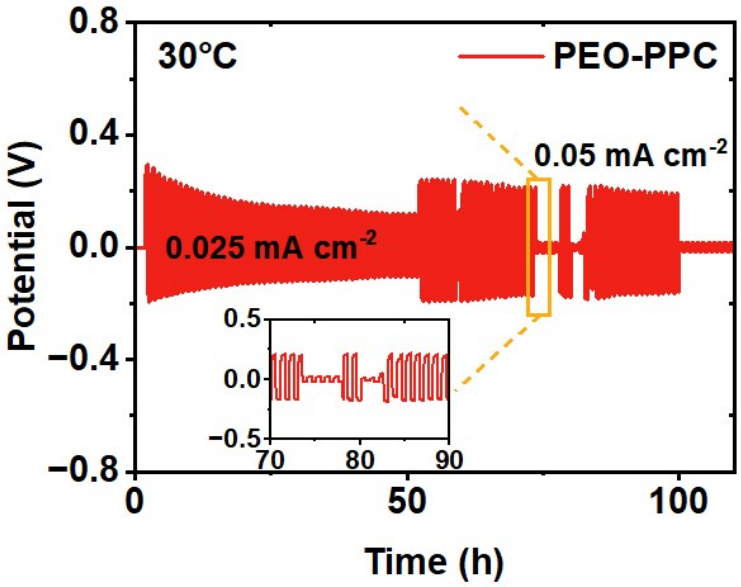

Figure S28. Voltage profiles of the continued lithium plating/stripping cycling of symmetric cells with PEO-PPC at current density of 0.025 mA cm^{-2} and 0.05 mA cm^{-2}.

Notes and references

1 Y. N. Zhou, Z. Xiao, D. Han, L. Yang, J. Zhang, W. Tang, C. Shu, C. Peng and D. Zhou, Adv. Funct. Mater., 2022, **32**, 2111314.

2 C. Wang, H. Zhang, J. Li, J. Chai, S. Dong and G. Cui, J. Power Sources, 2018, **397**, 157-161.

3 Q. Zhang, X. Zhang, J. Wan, N. Yao, T. Song, J. Xie, L. Hou, M. Zhou, X. Chen, B. Li, R. Wen, H. Peng, Q. Zhang and J. Huang, Nat. Energy, 2023, **8**, 725-735.

4 Q. K. Zhang, S. Y. Sun, M. Y. Zhou, L. P. Hou, J. L. Liang, S. J. Yang, B. Q. Li, X. Q. Zhang and J. Q. Huang, Angewandte Chemie International Edition, 2023, **62**, e202306889.

5 M. Wu, M. Li, Y. Jin, X. Chang, X. Zhao, Z. Gu, G. Liu and X. Yao, J. Energy Chem., 2023, **79**, 272-278.

6 J. Zhang, H. Zhang, R. Li, L. Lv, D. Lu, S. Zhang, X. Xiao, S. Geng, F. Wang, T. Deng, L. Chen and X. Fan, J. Energy Chem., 2023, **78**, 71-79.